

Synthesis, Identification, and Biological Evaluation of Some Metal Ions Complexes Derived from Thymine-Azo Ligand

Tabarak Taha Mizher* and Alyaa Khider Abbas

Department of Chemistry, College of Science, University of Baghdad, Al-Jadriya Street, Baghdad 10071, Iraq

* Corresponding author:

email:

tabarak.taha2305@sc.uobaghdad.edu.iq

Received: January 11, 2025

Accepted: February 16, 2025

DOI: 10.22146/ijc.103682

Abstract: New series of Ag(I) and Cu(II) complexes with general formulas of Ag(AAT)(H₂O)]NO₃·H₂O and Cu(AAT)(H₂O)₃]Cl₂·H₂O from 6-((5-chloro-2-hydroxyphenyl)diazenyl)-5-methylpyrimidine-2,4(1H,3H)-dione (AAT) were synthesized. By using FTIR, UV-vis, MS, and ¹H-NMR, their molecular structural and binding properties were confirmed, which indicated that the AAT ligand acts as a neutral tridentate O, N, and N, forming tetrahedral geometry with Ag-AAT and distorted octahedral with Cu-AAT. Additionally, C.H.N analysis, magnetic susceptibility, molar conductivity, and thermal analysis were used to identify the synthesized compounds' stability and molecular formula and explore their physical and chemical properties. XRD and AFM were also examined, where the ligand and Cu(II) complex exhibited nanoscale properties. The biological potential of these compounds was also investigated by testing their antioxidant activity. Furthermore, the Cu(II) complex was investigated for its effects on liver function and histological abnormalities in male albino rats. The enzymatic activities of liver markers such as glutamic-oxaloacetic transaminase, glutamic-pyruvate transaminase, and alkaline phosphatase were measured to determine the hepatoprotective properties. Histological investigations of liver tissues revealed further evidence for the biological effects of the copper compound. These results revealed the potential applications of Ag(I) and Cu(II) complexes derived from the thymine-azo ligand.

Keywords: antioxidant; histological activity; spectroscopic study; thymine-azo ligand

■ INTRODUCTION

The liver is the primary organ responsible for detoxifying the body, but it is continually exposed to free radicals produced by metabolic processes. When oxidative stress levels rise, liver cells are destroyed, releasing ALT and AST enzymes into the bloodstream, which indicates liver damage. Antioxidants, including glutathione, vitamins C and E, shield liver cells from free radical damage, which can worsen liver damage and cause elevated liver enzymes in conditions like cirrhosis, hepatitis, and fatty liver [1]. Research on antioxidants in blood and tissues can help determine the severity of oxidative stress and its role in these diseases. Antioxidants may assist in preventing liver damage and increase liver enzyme levels. Improving diet and boosting antioxidant intake can have a beneficial influence on liver health [2].

Therefore, studying liver enzymes and antioxidants combined provides a comprehensive picture of liver health, allowing for the determination of the level of oxidative stress and the development of appropriate treatments.

The design and synthesis of various azo derivatives containing heterocyclic moieties have been widely investigated for their applications in diverse fields, including optics, electrochemistry, and biology [3]. These compounds have been shown to enhance the performance of energy storage devices, sensors, and pharmaceuticals [4-5]. On the other hand, azo ligands, containing the active -N=N- group, exhibit a high propensity to coordinate with metal ions in various oxidation states. Synthetic and complexes of azo with transition and non-transition metals have been reported

to possess significant antifungal, antimicrobial, and anticancer properties, while displaying low toxicity to healthy cells [6-9].

Interestingly, thymine, an essential DNA and RNA building block, plays a critical role in biological processes. It existed in DNA as a methylated derivative of uracil, which is otherwise found in RNA. Thymine forms critical derivatives such as dTMP, dTDP, and dTTP, where the sugar present is deoxyribose. These compounds are integral to DNA synthesis and repair, underscoring the biological significance of thymine. Combining thymine's biological importance with azo compound properties opens new avenues for biomedical research [10].

This project aimed to synthesize and identify a new AAT ligand with its Ag(I) and Cu(II) complexes, these compounds were identified by several techniques such as FTIR, UV-vis, $^1\text{H-NMR}$, MS, C.H.N, magnetic susceptibility, molar conductance, thermal analyses (TGA/DTA), XRD and AFM. The antioxidant activity, histological activity, and effect of liver enzyme (glutamic-pyruvate transaminase (GPT), glutamic-oxaloacetic transaminase (GOT), and alkaline phosphatase (ALP)) of Cu-complex were examined.

■ EXPERIMENTAL SECTION

Materials

All chemicals and solvents were used of reagent grade, and no further purification containing sodium hydroxide, sodium nitrate, silver nitrate, copper chloride dihydrate, thymine, and 2-amino-4-chloro phenol.

Instrumentation

We employed C.H.N analysis to assess the elemental compositions of the AAT ligand and its complexes using an Eire EA 3000 Elemental Analyzer. The pH of the samples was tested with HANNA equipment. The FTIR spectra were measured using the SHIMADZU 8400 spectrophotometer. The UV-vis spectra for all studied chemicals were analyzed with a SHIMADZU 1800 UV-vis spectrophotometer. TGA was conducted using S.D.T., Q600 V20.9 Build to ascertain the metal content in the synthesized ligands and complexes. The molar

conductance of the metal ion complexes was measured in deionized water at a concentration of 0.001 M.

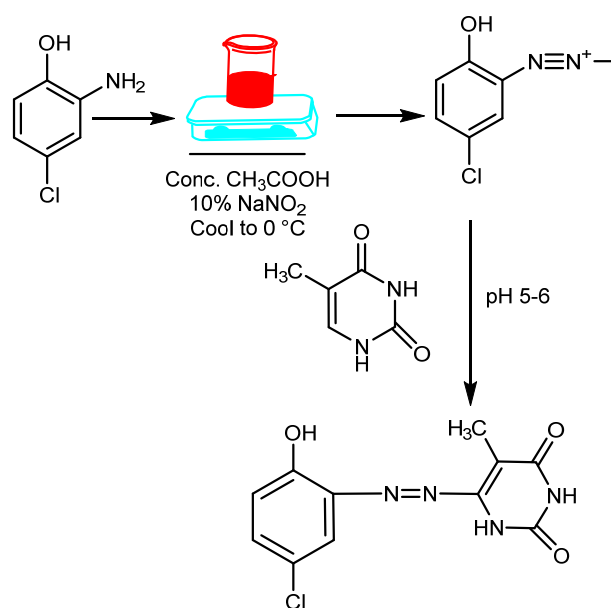
Procedure

Synthesis of AAT ligand

The new mono azo ligand (AAT) was prepared in a similar way in the literature [11], with some modifications and according to diazonium-coupling reaction where 1.436 g (0.01 M) of 2-amino-4-chloro phenol as primary amine was utilized to prepare the diazonium salt, while 1.26 g (0.01 M) thymine as coupling, The mixture was balanced to a pH of 5–6 by adding either acetic acid or sodium hydroxide. Then, the brown solid was filtered out and rinsed with a mix of distilled water and ethanol in equal parts before being collected and dried (Scheme 1).

Synthesis of AAT complexes

AAT complexes were formed with a mol ratio of 1:1 (M:L) by initially dissolving the ligand AAT (0.280 g, 1 mmol) in a small quantity of ethanol. This solution was then gradually incorporated into an aqueous solution of the selected metal ions, which included 1 mmol of each from 0.1698 g of AgNO_3 and 0.170 g of $\text{CuCl}_2 \cdot 2\text{H}_2\text{O}$ while stirring. The mixture was heated for 2 h, and the reaction's progress was monitored using TLC with a solvent mixture



Scheme 1. Synthesis of the AAT ligand

of 0.8 mL methanol, 1.2 mL ammonia, and 0.4 mL butanol [12]. The colored mixture was left overnight to complete the precipitation. The precipitate was collected via filtration and dried. The route of preparation for the new complexes is presented in Scheme 2.

Antioxidant activity test

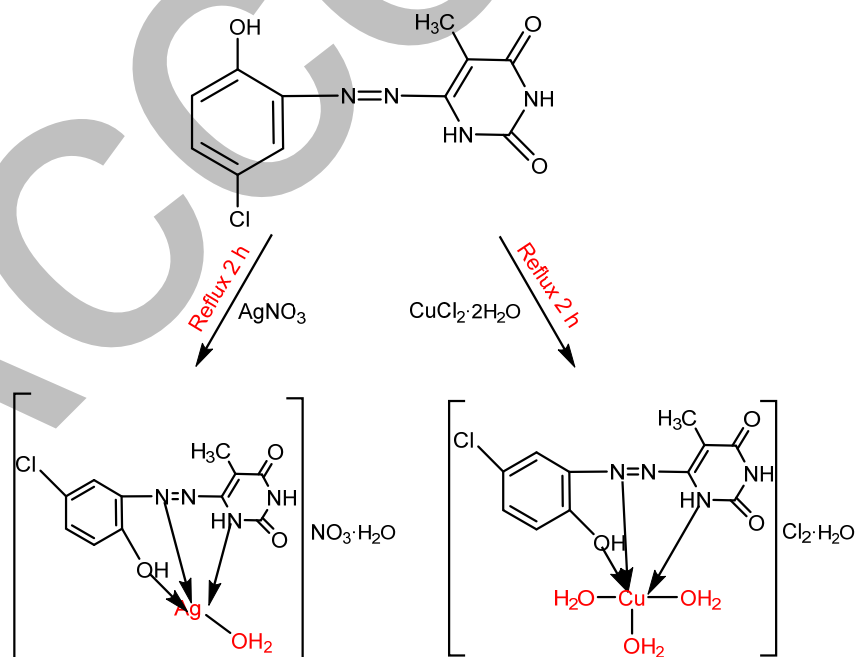
The total antioxidant capacity of the fractions was measured using the phosphomolybdate method, with ascorbic acid serving as the standard. A 0.1 mL sample solution at concentrations of 50, 100, and 150 mg/mL was combined with 1 mL of a reagent solution, which included 0.6 M sulfuric acid, 28 mM sodium phosphate, and 4 mM ammonium molybdate. The tubes were sealed and placed in a water bath at 95 °C for 90 min. Once the samples cooled to room temperature, we measured the absorbance of the mixture at 765 nm, comparing it to a blank. The blank consisted of 1 mL of the reagent solution and the right amount of ethanol, incubated under the same conditions. Ascorbic acid was used as the standard for comparison [13], an antioxidant capacity was estimated using the Eq. (1).

$$\text{Antioxidant effect (\%)} = \left[\frac{\text{control}_{\text{abs}} - \text{sample}_{\text{abs}}}{\text{control}_{\text{abs}}} \right] \times 100\% \quad (1)$$

Evaluation of hepatoprotective effects

The study looked at how certain substances protect the liver in albino male mice. The mice were between 8 to 10 weeks old and weighed between 23 to 27 g at the beginning of the experiments. The mice were placed into different groups, and each group was housed in its own plastic cage. The animals lived at room temperature and had unlimited access to food (standard pellets) and water. We measured certain enzymes in the serum, including GPT, GOT, and ALP, as well as examined liver tissue for any changes. We used a single dose of 200 mg/kg of $[\text{Cu}(\text{AAT})(\text{H}_2\text{O})_3]\text{Cl}_2 \cdot \text{H}_2\text{O}$ to study the effects in two groups of mice, with each group containing four mice. First, group I included mice received a single dose of 0.1 mL of distilled water for 14 d. Second, group II are mice received a single dose of 0.1 mL of 200 mg/kg of $[\text{Cu}(\text{AAT})(\text{H}_2\text{O})_3]\text{Cl}_2 \cdot \text{H}_2\text{O}$ for 14 d.

The materials that were tested were injected orally. Blood was taken from the heart using a puncture and placed into an Eppendorf tube, where it was allowed to clot at room temperature for 15 min. After that, the serum was separated by spinning it in a centrifuge at 3000 rpm for 10 min. This serum was later used to check



Scheme 2. preparing route of new complexes $[\text{Ag}(\text{AAT})(\text{H}_2\text{O})_2]\text{NO}_3$ and $[\text{Cu}(\text{AAT})(\text{H}_2\text{O})_3]\text{Cl}_2 \cdot \text{H}_2\text{O}$

liver function enzymes, including GOT, GPT, and ALP. Liver samples were collected and preserved in 10% formalin for histological studies [14].

The enzymatic activities of GPT and GOT in mouse serum were measured utilizing a commercial kit from Randox Company. The GPT activity (Unit/L) was derived from the standard curve provided by the kit. A specific kit from Bio Merieux Company was employed to assess ALP enzyme levels in mouse serum, following the conventional method [15]. This method involves hydrolysis of di-sodium phenyl phosphate, which releases phenol and produces sodium phosphate; the resulting phenol concentration is measured colorimetrically.

Preparation of liver tissue for histology

Each mouse's liver is prepared for a histological analysis utilizing the described procedure [16]. The samples are first fixed for 24 h in 10% formalin. They next go through a 5-min dehydration process using a series of alcohol solutions ranging from 30 to 100%. After being cleaned in two xylene changes, the samples are then embedded in paraffin wax for sectioning. Based on the established protocols, haematoxylin (Harison) and eosin are used to produce and stain 5-mm-thick cross sections. Under a light microscope, histopathological alterations are inspected and contrasted with the control group [17].

■ RESULTS AND DISCUSSION

General Concept

The obtained compounds are stable in air and have identical hues. Solubility tests revealed that they are soluble in absolute ethanol. AAT ligand was produced by combining an alkaline ethanoic solution of thymine

coupling with 2-amino-4-chlorophenol as a diazonium salt (Scheme 1). The value of molar conductivity for the produced metal indicates (1:1) electrolyte characteristic of Ag-AAT complex and (1:2) electrolyte of the Cu-AAT complex [18]. The entire spectroscopic and thermal gravimetric data are reported in the experimental section and in Table 1. The experimental data is in good accord with that derived theoretically.

Thermal Analysis

Fig. S1 shows how the synthesized AAT ligand and its complexes behave when heated. The thermal analyses were carried out with inert argon gas to prevent any oxidation or reduction of the complexes that were made. Meanwhile, Table 2 lists the expected and actual weight losses during different stages. The AAT ligand breaks down in four exothermic phases as the temperature rises from 25 to 1000 °C. The first decomposition phase happens between 25 and 160 °C, causing a 23.18% loss in weight. The second phase occurs from 160 to 265 °C, resulting in a 14.59% weight loss. The third phase takes place between 265 and 350 °C, leading to a 3.851% weight loss. The fourth phase starts at 350 °C and goes up to 520 °C, with a weight loss of 12.93% (as shown in Fig. S1(a)). The last phase runs from 520 to 1000 °C, resulting in a 37.42% weight loss. The [Ag(AAT)(H₂O)]NO₃·H₂O complex breaks down into three steps (Fig. S1(b)). The first step occurs from 25 to 210 °C, causing a 9.467% weight loss due to the release of chelate water [19]. The second stage happens from 210 to 410 °C, with a weight loss of 9.976%. The final stage runs from 410 to 1000 °C, leading to a 29.88% weight loss [20]. In contrast, [Cu(ATT)(H₂O)₃]Cl₂·H₂O breaks down

Table 1. Physicochemical data for the ligand (AAT) and its complexes

Compounds (M.wt) (g/mol)	Color and λ_{\max} (nm)	M:L	Λ_m (S mol ⁻¹)	Elemental Analysis				
				Experimental%, Theoretical%				
				C	H	N	M	Cl
C ₁₁ H ₉ N ₄ O ₃ Cl (AAT) (280.50)	Orange 419	-	8.5	47.93 (47.05)	4.19 (3.20)	20.87 (19.90)	-----	12.35 (12.89)
[Ag(AAT)(H ₂ O)]NO ₃ ·H ₂ O (486.28)	Purple 498	1:1	64.5	26.13 (27.14)	2.60 (2.78)	2.31 (1.43)	12.81 (11.87)	12.51 (12.47)
[Cu(AAT)(H ₂ O) ₃]Cl ₂ ·H ₂ O (487.04)	Signal orange 453	1:1	83.4	26.38 (27.15)	4.19 (3.49)	12.32 (11.52)	19.89 (19.87)	15.42 (15.40)

Table 2. TGA data of the AAT ligand and their complexes

Compound Molecular formula M.wt (g/mol)	Step	Range of decomposition (°C)	Suggested fragment	Mass loss%	
				Calc%	Found%
AAT	1	25–160	H ₉ ClC _{1.6}	23.17	23.18
C ₁₁ H ₉ N ₄ O ₃ Cl (280.5)	2	160–265	C _{3.4}	14.58	14.59
	3	265–350	C _{0.8}	3.84	3.85
	4	350–520	C ₃	12.92	12.93
	5	520–1000	C _{2.2} N ₄ O _{1.5}	37.39	37.42
	Residue	> 1000	O _{1.5}		
[Ag(AAT)(H ₂ O)]NO ₃ ·H ₂ O	1	25–210	H ₂ O _{0.6} Cl	9.47	9.47
AgC ₁₁ H ₁₃ N ₅ O ₈ Cl (486.28)	2	210–410	C _{1.2} H ₁₁ O _{1.4}	9.98	9.97
	3	410–1000	C _{9.8} N ₂	29.87	29.88
	Residue	> 1000	AgNO ₃		
[Cu(AAT)(H ₂ O) ₃]Cl ₂ ·H ₂ O	1	25–100	H ₆ O	5.10	5.11
CuC ₁₁ H ₁₇ N ₄ O ₇ Cl ₂ (486.04)	2	100–180	H ₂ O _{1.4}	5.09	5.09
	3	180–260	Cl _{0.4} O _{0.6}	4.59	4.60
	4	269–430	H ₉ Cl _{1.2}	10.50	10.51
	5	430–620	Cl _{0.4} C _{3.6}	11.11	11.12
	6	620–790	C _{7.4}	18.36	18.37
	7	790–1000	Cu _{0.2} N ₄ O ₃	23.35	23.36
	Residue	> 1000	Cu _{0.8}	25.94	

into seven parts (Fig. S1(c)). The first decomposition phase takes place between 25 to 100 °C, resulting in a 5.105% weight loss due to the loss of lattice water. The second phase occurs between 100 and 180 °C, where water molecules are lost. The third phase takes place from 180 to 260 °C and shows a weight loss of 4.604%. In the fourth phase, there is a weight loss of 10.51% from 260 to 430 °C. The fifth phase results in an 11.12% weight loss between 430 and 620 °C. During the sixth phase, from 620 to 790 °C, there is an 18.37% weight loss. Finally, between 790 to 1000 °C, the weight loss reaches 23.36% [21-22].

Mass Spectroscopy

Mass spectrometry (MS) is one of the most powerful modern physical-chemical methods for identifying compounds and studying their structure and reactivity [23-24]. The suggested formula of the AAT ligand was emphasized by the different obtained molecular ion peaks at various intensities, base peaks, and other fragments. Scheme 3 and Fig. S2 showed the molecular ion peak at $m/z = 280.1$, which confirmed the formation of the AAT

ligand, and the base peak was found at $m/z = 80.0$ with a high intensity.

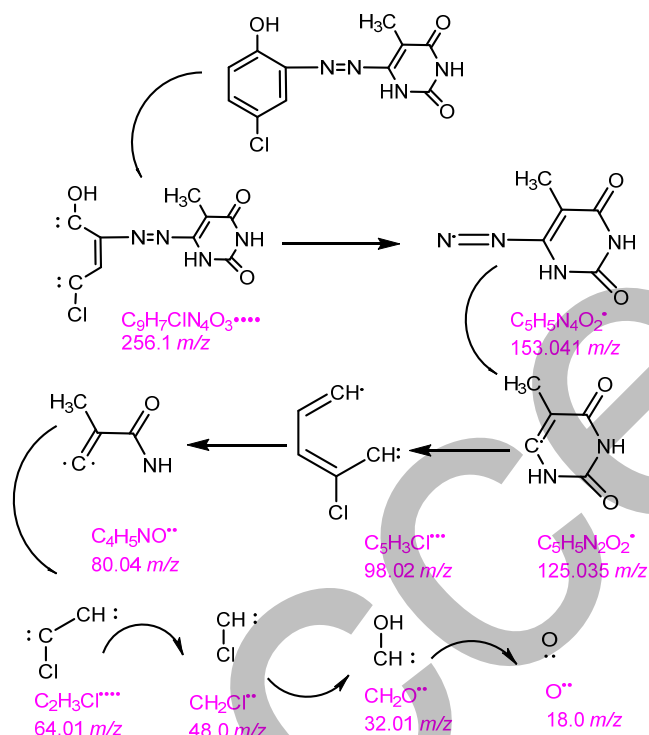
FTIR Spectra

FTIR spectra can aid in predicting the chelating mechanism of the AAT ligand with metal ions in the synthesized complexes. Table 3 lists the most important stretching vibration band of functional moieties that took part in the chelating, the $\nu(\text{OH})$ and $\nu(\text{NH})$ were changed in shape and disappeared respectively after complex formation, which indicated the chelation via these moieties (Fig. S3(a-c)) [25]. The band associated with $\nu(\text{C}=\text{O})$ remained unchanged in the complex spectra, this notice confirms the non-participation of this moiety with a chelating ring [26-28]. However, the higher change in positions and intensity of the $\nu(\text{N}=\text{N})$ and $\nu(\text{C}-\text{N}=\text{N}-\text{C})$ moieties can be related to the chelating of nitrogen azo moiety with metal ion [29-30]. Additionally, several new bands not observed in the free-ligand spectrum were detected, particularly significant changes occurring in the 405–690 cm^{-1} range. These bands

Table 3. Vibration bands for ligand (AAT) and its complexes

Compounds	$\nu(\text{OH})$	$\nu(\text{NH})$	$\nu(\text{C}=\text{O})$	$\nu(\text{N}=\text{N})$	$\nu(\text{C}-\text{N}=\text{N}-\text{C})$	$\nu(\text{M}-\text{N})$	$\nu(\text{M}-\text{N})$	$\nu(\text{M}-\text{O})$	$\nu(\text{M}-\text{OH})$
						prm	azo	H_2O	H_2O
AAT	3434 3460 d	3180	1704 1687 d	1510 1558 T 1568	1230 sh	-----	-----	-----	-----
[Ag(AAT)(H ₂ O)]NO ₃ ·H ₂ O	3450 3433 3402 T, br	-----	1681 vw	1556 vw	1247 vw	659	576 w	422 w 478	549
[Cu(AAT)(H ₂ O) ₃]Cl ₂ ·H ₂ O	3523 3444 3413 T, br	-----	1681 vw	1575 w	1325 Sh	678 sh	551	422 vw 451	551

m = medium, w = weak, sh = sharp, prm = pyrimidine, vw = very weak, d = doublet, T= triplet

**Scheme 3.** Fragmentation of AAT ligand

in this region are likely associated with the stretching absorptions of M–N azo and M–N prm, as well as M–O(H₂O) and M–OH. This supports our findings concerning the chelation sites of the ligands with metal

ions. Based on this information AAT ligand acts as a neutral N, N, O-tridentate ligand, forming a penta-chelating ring [31].

UV-vis of AAT Ligand and Their Complexes

The UV-vis spectra of the AAT and its complexes have been taken in absolute ethanol (10^{-4} M) in the scan range of 250–1100 nm. The AAT showed two bands at 291 (34364 cm^{-1}) and 412 nm (24096 cm^{-1}) because of $\pi \rightarrow \pi^*$ and $n \rightarrow \pi^*$ electronic transitions via N=N, C=O, and OH moieties as well as benzene ring [32]. The tetrahedral geometry of d¹⁰ of silver complex exhibited a red shift with a charge transfer band (C.T) at 496 nm (20161 cm^{-1}) as a result of the coordination and consequently diamagnetic nature. The geometry of the copper complex is a distorted octahedral and has a shoulder band at 505 nm (19801 cm^{-1}) which is reversed to ${}^2E_g \rightarrow {}^2T_g$ transition [33–34]. The UV-vis spectra is presented in Fig. S4 and summarized in Table 4.

¹H-NMR of AAT Ligand

The ¹H-NMR analysis reveals that the compound possesses various distinct functional groups, including OH moiety at 9.41 ppm, N–H amide at 9.38 ppm, and a CH₃ moiety at 2.34 ppm [35], while aromatic protons are

Table 4. Electronic spectra for the AAT ligand and their complexes

Compounds	Peak (nm)	Wavenumber (cm^{-1})	Assignment	Hybridization	Geometry	μ_{eff} (B.M)
AAT	291 412	34364 24096	$\pi \rightarrow \pi^*$ $n \rightarrow \pi$	-----	-----	Dia
[Ag(AAT)(H ₂ O)]NO ₃ ·H ₂ O	496	20161	CT	sp ³	Tetrahedral	Dia
[Cu(AAT)(H ₂ O) ₃]Cl ₂ ·H ₂ O	505	19801	${}^2E_g \rightarrow {}^2T_g$	sp ³ d ²	Distorted octahedral	1.87

found in the range of 7.67 to 7.70 ppm. The downfield shifts of the OH and NH groups are due to deshielding effects from electronegative atoms and possible hydrogen bonding, whereas the shift of the methyl group suggests its proximity to an electron-withdrawing carbonyl group (Fig. S5) [36].

X-Ray Diffraction

The three key reflection peaks for the AAT and [Cu(AAT)(H₂O)₃]Cl₂·H₂O fall within the 2θ ranges of 13.34–27.14° and 31.77–45.49°, respectively. This data indicates that the semi-crystalline structure and particle size of the AAT ligand and its Cu(II) complexes can be assessed through XRD patterns by examining the most intense peak relative to other reflections, using the Renewed Debye-Teller method [37]. The prominent reflection peak for the AAT ligand is located at 13.34°, while the peak for [Cu(AAT)(H₂O)₃]Cl₂·H₂O appears at 31.77°.

The formula for calculating the main size of crystalline domains (D) is given by the Eq. (2);

$$D = K\lambda / \beta \cos \theta \quad (2)$$

where, D refers to the size of crystalline domains, which may be equal to or smaller than the crystal grain size (the apparent particle size of the grains) and is expressed in volume units (Å) or nanometers (nm). β denotes the full width at half maximum (FWHM) of the XRD peak. θ is the Bragg angle, λ equals to 0.15406 nm, and K is a constant (0.9). This text highlights the XRD data, suggesting that the particle size is in the nanoscale range. The interplanar spacing (d) was calculated using the intense peak position following Bragg's in Eq. (3) [38];

$$n\lambda = 2d \sin \theta \quad (3)$$

where λ = 0.15406 Å, n is the integer number, d is the spacing between crystal layers (the path difference), and θ is the incident angle (the angle between the incoming ray and the scattering plane). Table 5 shows the summary of the XRD data for all compounds, and the XRD spectra is presented in Fig. S6.

AFM Analysis

AFM analysis is a type of scanning electron microscope used to investigate material surface properties at the nanoscale. The contract of atoms in AFM analysis images was mostly determined by each element's van der Waals radius [39-40]. For the AAT, the AFM image (Fig. S7) appeared less rough with content of Sp = 144.7 nm and Sv = 26.28 nm. In comparison, those of Cu(II) complex (Sp = 193 nm and Sz = 256.7 nm), as depicted in Fig. S8, showed relatively greater surface roughness and development of domains of various shapes and sizes. On the other hand, the grain sizes powder different areas of the ligand AAT and Cu(II) complex were shown in the Fig. S8 by utilizing threshold detection with a coverage of 29.61 and 27.14%, respectively.

Antioxidant Capacity

The antioxidant capacity of the AAT ligand and their complexes as well as ascorbic acid as standard. The data obtained detected that the antioxidant capacity will be increased with an increase in concentration for all synthesized compounds (Table 6). Fig. S9 manifested that Cu-complex has the highest antioxidant capacity at 150 µg/mL than Ag-complex and the AAT ligand.

Hepatoprotective Activity

Liver function tests are blood tests that assist in determining the cause of symptoms and tracking the status of liver disease or damage. These tests assess the levels of specific enzymes and proteins in the blood. Some evaluate how effectively the liver performs its regular functions, such as producing protein and eliminating bilirubin, a waste product. Other liver function tests focus on the enzymes produced by liver cells in reaction to injury or disease [41].

The data improved the activity of liver enzymes, phosphatase ALK, GOT, and GPT, under two conditions: a negative control and treatment with a copper

Table 5. All data of X-ray diffraction for AAT and [Cu(ATT) (H₂O)₃]Cl₂·H₂O

Compounds	2θ (°)	FWHM (nm)	D (nm)	d (Å)	
				Calculated	Found
ATT	13.34	0.240	0.389	6.644	6.632
[Cu(ATT)(H ₂ O) ₃]Cl ₂ ·H ₂ O	31.77	0.157	0.953	2.816	2.814

Table 6. Antioxidant activity of AAT, Ag, and Cu complexes

Sample No.	150 µg/mL		100 µg/mL		50 µg/mL	
	Absorbance	Conc.	Absorbance	Conc.	Absorbance	Conc.
Control	0.133 ± 0.002	20.11	0.124 ± 0.002	18.75	0.144 ± 0.002	17.31
AAT	0.096 ± 0.003	14.51	0.059 ± 0.003	8.94	0.030 ± 0.003	4.47
[Ag(AAT)(H ₂ O)]NO ₃ ·H ₂ O	0.091 ± 0.003	13.82	0.049 ± 0.003	7.42	0.000	0.00
[Cu(AAT)(H ₂ O) ₃]Cl ₂ ·H ₂ O	0.107 ± 0.004	16.21	0.067 ± 0.004	10.15	0.028 ± 0.003	4.24

complex, [Cu(AAT)(H₂O)₃]Cl₂·H₂O. Below is a further breakdown (ALK) as negative control (173 ± 2.517), which indicates the baseline ALK activity in the liver when not treated. In contrast, when treated with [Cu(AAT)(H₂O)₃]Cl₂·H₂O (168 ± 2.517), there is a slight decrease in ALK activity with the copper complex treatment. This change is minimal and likely falls within the margin of experimental error, and this implies the complex has a negligible impact on ALK activity and does not significantly affect liver bile function or alkaline phosphatase production, the activity of GOT of negative control (28 ± 1.271), and for [Cu(AAT)(H₂O)₃]Cl₂·H₂O (36 ± 1.510): Treatment at the Cu(II) complex resulted in an increased GOT level, suggesting slight hepatocellular stress or injury. Although the rise is not severe, it points to some extent of liver cell damage or metabolic disruption caused by the compound. The results of 21 ± 1.000 for GPT implies that this value represents the baseline of GPT activity, a more specific marker for liver health compared to GOT, the negative control for [Cu(AAT)(H₂O)₃]Cl₂·H₂O complex (25 ± 1.732). Similarly, GPT levels rise moderately after treatment, indicating potential damage to liver cell membranes or changes in liver metabolism due to the Cu(II) complex exposure.

Histopathological Activity of the Liver

The liver histopathological data are used for control treatment and with [Cu(AAT)(H₂O)₃]Cl₂·H₂O were illustrated in Fig. S10 and S11. When treated with Cu(II) complex, the liver's histopathological feature showed mild congestion of the central vein and proliferation figures of the hepatocytes and inculcated hepatocytes with a normal arrangement of hepatic cords (Fig. S11).

CONCLUSION

This research successfully synthesized and characterized new Ag(I) and Cu(II) complexes using the AAT ligand. Structural analysis revealed that the AAT ligand functions as a neutral tridentate (O, N, N) donor. C.H.N analysis, magnetic susceptibility, molar conductivity, and thermal analysis, further substantiated the complexes' proposed molecular structures and stability. XRD and AFM indicated nanoscale characteristics of both the ligand and the Cu(II) complex. The biological evaluation revealed significant antioxidant properties, while the Cu(II) complex was additionally examined for its impact on liver function in male albino rats. Enzymatic tests for GPT, GOT, and ALP suggested possible hepatotoxic or hepatoprotective effects, supported by histological examinations of liver tissues. These results imply potential biomedical applications, especially for the copper complex. Nonetheless, additional research is required to clarify the mechanisms behind its biological activity.

ACKNOWLEDGMENTS

The authors thank the University of Baghdad for supporting this research project.

CONFLICT OF INTEREST

There are no conflicts of interest to declare.

AUTHOR CONTRIBUTIONS

Tabarak Taha Mizher and Alyaa Khider Abbas contributed to research design, conduct the experimental work, interpret the results, and draft the manuscript. All authors reviewed and approved the final version of the manuscript.

■ REFERENCES

- [1] Lee, T.H., Kim, W.R., and Poterucha, J.J., 2012, Evaluation of elevated liver enzymes, *Clin. Liver Dis.*, 16 (2), 183–198.
- [2] Abdalah, M.E., Al-Ezzy, R.M., and Okhti, Z.A., 2018, Protective role of *Viola odorata* against hepatotoxicity induced by methotrexate in albino male mice, *J. Pharm. Sci. Res.*, 10 (11), 2775–2782.
- [3] Manhee, T.Q., and Alabdali, A.J., 2024 Synthesis, characterization and anticancer activity of Ni(II), Cu(II), Pd(II) and Au(III) complexes derived from novel Mannich base, *Vietnam J. Chem.*, 62 (2), 201–210.
- [4] Maliyappa, M.R., Keshavayya, J., Mahanthappa, M., Shivaraj, Y., and Basavarajappa, K.V., 2020, 6-Substituted benzothiazole based dispersed azo dyes having pyrazole moiety: Synthesis, characterization, electrochemical and DFT studies, *J. Mol. Struct.*, 1199, 126959.
- [5] Matada, M.N., Jathi, K., Malingappa, P., and Pushpavathi, I., 2020, Synthesis, spectroscopic, DFT and electrochemical studies of heterocyclic azo dyes derived from 1-[(E)-benzylideneamino](phenyl)methyl} naphthalen-2-ol, *Chem. Data Collect.*, 25, 100314.
- [6] Abdnoor, Z.M., and Alabdali, A.J., 2019, Synthesis, characterization, and anticancer activity of some azole-heterocyclic complexes with gold(III), palladium(II), nickel(II), and copper(II) metal ions, *J. Chin. Chem. Soc.*, 66 (11), 1474–1483.
- [7] Gaber, M., Fathalla, S.K., and El-Ghamry, H.A., 2019, 2,4-Dihydroxy-5-[(5-mercapto-1H-1,2,4-triazole-3-yl)diazenyl]benzaldehyde acetato, chloro and nitrate Cu(II) complexes: Synthesis, structural characterization, DNA binding and anticancer and antimicrobial activity, *Appl. Organomet. Chem.*, 33, e4707.
- [8] Saad, F.A., El-Ghamry, H.A., and Kassem, M.A., 2019, Synthesis, structural characterization and DNA binding affinity of new bioactive nano-sized transition metal complexes with sulfathiazole azo dye for therapeutic applications, *Appl. Organomet. Chem.*, 33 (7), e4965.
- [9] El-Deen, I.M., Shoair, A.F., and El-Bindary, M.A., 2019, Synthesis, characterization and biological properties of oxovanadium(IV) complexes, *J. Mol. Struct.*, 1180, 420–437.
- [10] Khan, M.N., Parmar, D.K., and Das, D., 2021, Recent applications of azo dyes: A paradigm shift from medicinal chemistry to biomedical sciences, *Mini-Rev. Med. Chem.*, 21 (9), 1071–1084.
- [11] Abbas, A.K., 2022, Synthesis, spectroscopic, thermal and biological studies of some novel metal ions complexes, *MINAR Int. J. Appl. Sci. Technol.*, 4 (3), 331–348.
- [12] Ullah, Q., Khan, S.A., and Mohammad, A., 2021, Applications of green solvents in thin-layer chromatography (TLC)—An overview, *J. Planar Chromatogr. - Mod. TLC*, 34 (1), 5–29.
- [13] Thilagavathi, T., Kathiravan, G., and Srinivasan, K., 2016, Antioxidant activity and synthesis of silver nanoparticles using the leaf extract of *Limonia acidissima*, *Int. J. Pharma Bio Sci.*, 7, 201–205.
- [14] Al-Ezzy, R.M., Hassan, Z.Y.M., and Al-Jumaili, F.T.O., 2016, Hematological toxic effect and the frequency of micronucleus formation of different doses of cyproheptadine on albino male mice blood picture, *Iraqi J. Hematol.*, 5 (2), 149–153.
- [15] Al-Ezzy, R.M., Al Anee, R.S.A., and Kathum, O.A., 2017, Hepatoprotective effects of *Achillea millefolium* methanolic extract on carbon tetrachloride induced hepatotoxicity on albino male mice, *Int. J. Adv. Res. Biol. Sci.*, 4 (8), 98–109.
- [16] Ibrahim, N.A., Al-Shmgani, H.S., and Ibrahim, R., 2017, Cytarabine induced reproductive histopathological changes in albino male mice, *J. Biotechnol. Res. Cent.*, 11 (1), 6–12.
- [17] Al-Ezzy, R.M., Soud, S.A., and Sadoon, Z.M., 2019, Histopathological study and oxidative stress, antioxidants parameters and liver enzymes activity determination of *Cyperus* methanolic extract and glucophage drug on albino male mice, *Am. J. Biosci. Bioeng.*, 7 (1), 10–15.
- [18] Salih, B.D., Dalaf, A.H., Alheety, M.A., Rashed, W.M., and Abdullah, I.Q., 2021, Biological activity and laser efficacy of new Co(II), Ni(II), Cu(II),

- Mn(II) and Zn(II) complexes with phthalic anhydride, *Mater. Today: Proc.*, 43, 869–874.
- [19] Mallikarjuna, N.M., Keshavayya, J., Maliyappa, M.R., Shoukat Ali, R.A., and Venkatesh, T., 2018, Synthesis, characterization, thermal and biological evaluation of Cu(II), Co(II) and Ni(II) complexes of azo dye ligand containing sulfamethazole moiety, *J. Mol. Struct.*, 1165, 28–36.
- [20] Abbas, A.K., and Fadhil, A.E., 2024, Preparation, structural identification, and biomedical evaluation of some new complexes, *Indones. J. Chem.*, 24 (6), 1730–1742.
- [21] Gaber, M., El-Wakiel, N., and Hemeda, O. M., 2019, Cr(III), Mn(II), Co(II), Ni(II) and Cu(II) complexes of 7-((1*H*-benzo[*d*]imidazol-2-yl)diazenyl)-5-nitroquinolin-8-ol. synthesis, thermal, spectral, electrical measurements, molecular modeling and biological activity, *J. Mol. Struct.*, 1180, 318–329.
- [22] Abbas, A.K., 2015, Lanthanide ions complexes of 2-(4-amino antipyrine)-*L*-tryptophane (AAT): Preparation, Identification and Antimicrobial Assay, *Iraqi J. Sci.*, 56 (4c), 3297–3309.
- [23] Noriega, P., Gortaire, G., and Osorio, E., 2022, “Mass Spectrometry and Its Importance for the Analysis and Discovery of Active Molecules in Natural Products” in *Natural Drugs from Plants*, Eds. El-Shemy, H., IntechOpen, Rijeka, Croatia.
- [24] Hammada, R.G., and Shaalan, N., 2024, Synthesis, spectroscopy and biological activity study of some new complexes with Schiff base derived from malonic acid dihydrazide with 2-pyridine carboxaldehyde, *Baghdad Sci. J.*, 21 (5), 1577–1591.
- [25] Hussein, K.A., Shaalan, N., Lafta, A.K., and Al Akeedi, J.M., 2024, Preparation, characterization, and biological activity of La(III), Nd(III), Er(III), Gd(III), and Dy(III) complexes with Schiff base resulted from reaction of 4-antipyrinecarboxaldehyde and 2-aminobenzothiazole, *Indones. J. Chem.*, 24, 358–369.
- [26] Prakash, S., Somiya, G., Elavarasan, N., Subashini, K., Kanaga, S., Dhandapani, R., Sivanandam, M., Kumaradhas, P., Thirunavukkarasu, C., and Sujatha, V., 2021, Synthesis and characterization of novel bioactive azo compounds fused with benzothiazole and their versatile biological applications, *J. Mol. Struct.*, 1224, 129016.
- [27] Masoud, M.S., Ali, A.E., Elasala, G.S., and Kolkaila, S.A., 2017, Spectroscopic studies and thermal analysis on cefoperazone metal complexes, *J. Chem. Pharm. Res.*, 9 (4), 171–179.
- [28] Al-Lami, N.J., 2015, New imidazo[2,1-*b*]naphtha[2,1-*d*][1,3]thiazole derivatives: Synthesis, antimicrobial and antifungal activity, *Iraqi J. Sci.*, 56 (4c), 3274–3284.
- [29] Bouhdada, M., and EL Amame, M., 2017, Synthesis, characterization and spectroscopic properties of the hydrazodye and new hydrazodye-metal complexes, *J. Mol. Struct.*, 1150, 419–426.
- [30] Patel, K.D., and Patel, H.S., 2017, Synthesis, spectroscopic characterization and thermal studies of some divalent transition metal complexes of 8-hydroxyquinoline, *Arabian J. Chem.*, 10, S1328–S1335.
- [31] Štoček, J.R., and Dračinský, M., 2020, Tautomerism of guanine analogues, *Biomolecules*, 10 (2), 170.
- [32] Mahmoud, W.A., Ali, A.A.M., and Kareem, T.A., 2015, Preparation and spectral characterization of new azo imidazole ligand 2-[(2'-cyano phenyl) azo]-4,5-diphenyl imidazole and its complexes with Co(II), Ni(II), Cu(II), Zn(II), Cd(II) and Hg(II) ions, *Baghdad Sci. J.*, 12 (1), 96–109.
- [33] Northridge, M.E., Kumar, A., and Kaur, R., 2020, Disparities in access to oral health care, *Annu. Rev. Public Health*, 41, 513–535.
- [34] Ali, A.A., Al-Hassani, R.M., Hussain, D.H., Rheima, A.M., and Meteab, H.S., 2020, Synthesis, spectroscopic, characterization, pharmacological evaluation, and cytotoxicity assays of novel nano and micro scale of copper(II) complexes against human breast cancer cells, *Drug Invent. Today*, 14 (1), 31–39.
- [35] Hessoon, H.M., and Abbas, H.M., 2024, Synthesis and characterization of a novel dapsone-derived bisazo ligand and its gold(III) complex, with evaluation of its antioxidant and anticancer activities, *Indones. J. Chem.*, 24 (2), 481–491.

- [36] Claridge, T.D.W., 2016, *High-Resolution NMR Techniques in Organic Chemistry*, 3rd Ed., Elsevier, Radarweg, Amsterdam, Netherlands.
- [37] Basak, M., Rahman, M.F., Ahmed, M.F., Biswas, B., and Sharmin, N., 2022, The use of X-ray diffraction peak profile analysis to determine the structural parameters of cobalt ferrite nanoparticles using Debye-Scherrer, Williamson-Hall, Halder-Wagner and Size-strain plot: Different precipitating agent approach, *J. Alloys Compd.*, 895, 162694.
- [38] Stepanov, S., 2021, New developments including X-ray standing waves in the dynamical Bragg diffraction program of X-ray server, *J. Appl. Crystallogr.*, 54, 1530–1534.
- [39] Bhushan, B., 2017, *Springer Handbook of Nanotechnology*, 4th Ed., Springer, Springer-Verlag GmbH, Germany.
- [40] Kosareva, E.K., Pivkina, A.N., and Muravyev, N.V., 2022, Atomic force microscopy in energetic materials research: A review, *Energy Mater. Front.*, 3 (4), 290–302.
- [41] Datta, S., Aggarwal, D., Sehrawat, N., Yadav, M., Sharma, V., Sharma, A., Zghair, A.N., Dhama, K., Sharma, A., Kumar, V., Sharma, A.K., and Wang, H., 2023, Hepatoprotective effects of natural drugs: Current trends, scope, relevance and future perspectives, *Phytomedicine*, 121, 155100.